Friction **11**(1): 76–92 (2023)
https://doi.org/10.1007/s40544-021-0575-4
ISSN 2223-7690
CN 10-1237/TH
RESEARCH ARTICLE

Insights into the tribological behavior of choline chloride–urea and choline chloride–thiourea deep eutectic solvents

Yuting LI[1], Yuan LI[1], Hao LI[1,*], Xiaoqiang FAN[1,*], Han YAN[1], Meng CAI[2], Xiaojun XU[1], Minhao ZHU[1,2]

[1] *Key Laboratory of Advanced Technologies of Materials (Ministry of Education), School of Materials Science and Engineering, Southwest Jiaotong University, Chengdu 610031, China*

[2] *Tribology Research Institute, School of Mechanical Engineering, Southwest Jiaotong University, Chengdu 610031, China*

Received:22 June 2021 / Revised: 01 August 2021 / Accepted: 20 November 2021

Abstract: Deep eutectic solvents (DESs) have been considered as novel and economic alternatives to traditional lubricants because of their similar physicochemical performance. In this study, choline chloride (ChCl) DESs were successfully synthesized via hydrogen-bonding networks of urea and thiourea as the hydrogen bond donors (HBDs). The as-synthesized ChCl–urea and ChCl–thiourea DESs had excellent thermal stability and displayed good lubrication between steel/steel tribo-pairs. The friction coefficient and wear rate of ChCl–thiourea DES were 50.1% and 80.6%, respectively, lower than those of ChCl–urea DES for GCr15/45 steel tribo-pairs. However, for GCr15/Q45 steel, ChCl–urea DES decreased the wear rate by 85.0% in comparison to ChCl–thiourea DES. Under ChCl–thiourea DES lubrication, the tribo-chemical reaction film composed of FeS formed at the interfaces and contributed to low friction and wear. However, under high von Mises stress, the film could not be stably retained and serious wear was obtained through direct contact of friction pairs. This illustrated that the evolution of the tribo-chemical reaction film was responsible for the anti-friction and anti-wear properties of the DESs.

Keywords: deep eutectic solvents (DESs); tribo-chemical film; von Mises stress; lubrication mechanism

1 Introduction

Lubricants can control friction, minimize the wear of mating surfaces, cool the contact surfaces, and prevent corrosion via the sealing effect, thus prolonging the service life of machines and conserving resources [1–3]. However, the disadvantages of lubricants, such as high cost, complicated synthesis, and environmental pollution, have gained attention in the lubrication industry amid growing environmental awareness [3, 4]. Therefore, there is an urgent requirement and challenge to develop high-performance and low-cost lubricants using a facile synthetic procedure.

Deep eutectic solvents (DESs) are an innovative type of green solvents that possess lower melting points than their constituent components [5, 6]. DESs are usually composed of hydrogen bond acceptors (HBAs) and hydrogen bond donors (HBDs) connected through hydrogen-bonding networks [7]. DESs share physicochemical properties with ionic liquids (ILs), such as non-flammability, low volatility, high electrical conductivity, and high thermal stability as well as customizability for desired applications [7–11]. The ease of synthesis, low cost, good biocompatibility, and non-toxicity are unique characteristics of DESs [7, 12, 13]. Therefore, they are being widely used in various applications including making CO_2 dissolution easily [14], dissolution of metal oxides [15], drug solubilization [16], purification of biodiesel [17], catalytic reactions [18], and lubrication [19]. The application of choline chloride (ChCl)-based DESs for lubrication was initiated by Abbott et al. [1, 19] in 2010s. They

* Corresponding authors: Hao LI, E-mail: lihao@swjtu.edu.cn; Xiaoqiang FAN, E-mail: fxq@home.swjtu.edu.cn

found that ChCl–ethylene glycol and ChCl–urea DESs provided lower friction coefficients than SAE 5W30 engine oil for steel/steel tribo-pairs [19]. Under high-speed/low-load conditions, the lubrication properties of the DESs were retained by increasing the surface roughness. They also studied the corrosion and wear resistances of water-miscible DESs, including ChCl–urea DES, ChCl–ethylene glycol DES, ChCl–glycerol DES, and ChCl–oxalic acid DES [1]. Surprisingly, some aqueous DESs showed low corrosion rates on steel, nickel, and aluminum, indicating their potential as marine lubricants [1]. The tribological performance of carbon fiber (CF)-filled polytetrafluoroethylene (PTFE) composites under ChCl-based DESs was much better than that under water and hydraulic oil [20]. The friction coefficient and wear rate of CF/PTFE composites lubricated by ChCl-based DESs were reduced by 60% and 50%, respectively, when compared with those obtained under the dry friction condition. The tribological properties of silicon surfaces lubricated by DESs formed by ionic liquids containing sulfonate anions and polyethylene glycol were studied using a nanotribometer [21]. The DESs exhibited good lubrication performance on the silicon surface. The lubrication properties of nanofilms of ChCl–ethylene glycol DESs between two mica surfaces were investigated by Hallet et al. [22]. DESs without and with a small amount of water exhibited low friction coefficient values at low loads, but increased to 0.12 at high loads. In summary, ChCl-based DESs show good tribological properties, which may be due to the formation of a friction film on the worn surface. However, systematic research on the tribological mechanism of DESs as lubricants is still lacking.

In this study, urea and thiourea with similar chemical structures were selected as HBDs to synthesize DESs. To reveal the tribological behaviors of ChCl-based DESs, we comprehensively probed the tribological responses of ChCl–urea and ChCl–thiourea DESs to substrates with different mechanical properties. The tribological mechanism was analyzed by energy-dispersive X-ray spectroscopy (EDS), X-ray photoelectron spectroscopy (XPS), and the finite element methods. This study aims to design DESs as high-performance but low-cost lubricants and to explore the tribological mechanism. It also lays the foundation and advances the broad applications for DESs serving as lubricants.

2 Experimental details

2.1 Synthesis of DESs

Choline chloride (ChCl, 98% purity), urea (99% purity), and thiourea (99% purity) were purchased from Chengdu Kelong Chemical Co., Ltd., China. All the reagents were used as-received without further purification. ChCl was dried under vacuum at 50 °C for 2 h prior to use. ChCl–urea DES was prepared by mixing ChCl with urea at a molar ratio of 1:2, followed by constant stirring for 1 h at 80 °C, forming a homogenous and colorless liquid. Similarly, ChCl and thiourea were mixed in a molar ratio of 1:2, followed by stirring at 120 °C for 0.5 h, to obtain a colorless transparent liquid of ChCl–thiourea DES.

2.2 Characterization of DESs

The chemical structures of the two DESs and their pure constituents were confirmed by the Fourier-transform infrared (FTIR) spectroscopy (Nicolet 6700, USA) of liquid film and KBr pellets in the wavenumber range of 400–4,000 cm^{-1}. The thermal stabilities of the DESs were evaluated by the thermogravimetric analysis meter (TGA; NETZSCH STA449F3, Germany) under nitrogen atmosphere from 20 to 500 °C at a heating rate of 20 °C/min. Differential scanning calorimetry (DSC; Waters Corporation 2500, USA) of ChCl–urea and ChCl–thiourea DESs were performed in nitrogen atmosphere at a heating rate of 10 °C/min from −80 to 50 °C and 20 to 100 °C, respectively. The viscosity of the DESs was measured using a kinematic viscometer (SYD-265, Dalian Wuzhou Petroleum Equipment Co., Ltd., China). To evaluate the wettability of ChCl–urea and ChCl–thiourea DESs, the contact angles were measured at 80 °C using an optical contact angle meter (OCA15EC, DataPhysics Co., Ltd., Germany).

2.3 Friction and wear tests

The tribological properties of ChCl–urea and ChCl–thiourea DESs were assessed at 80 °C using a reciprocating ball-on-disc tribometer. On account of the different hydrogen bond interactions between

HBDs and HBAs [2], ChCl–urea DES is a liquid, while ChCl–thiourea DES is a solid at 20 ± 2 °C. Therefore, the specimen stage was maintained at 80 °C during the friction tests. The substrates used in the experiments were 45 steel, and 45 steel quenched at 900 °C (Q45 steel). The average roughness values of 45 steel and Q45 steel are 23.6 and 28.1 nm, respectively. The tribo-pairs and chemical structures of the synthetic DESs are shown in Fig. 1 and listed in Table 1.

ChCl–urea DES (I) and ChCl–thiourea DES (II) correspond to the experiments conducted with a GCr15 steel ball sliding against 45 steel lubricated with ChCl–urea and ChCl–thiourea DESs, respectively. Meanwhile, ChCl–urea DES (III) and ChCl–thiourea DES (IV) correspond to the use of ChCl–urea DES and ChCl–thiourea DESs as lubricants for GCr15 steel/Q45 steel pairs, respectively.

The mechanical properties of the substrates were measured by the nanoindentation (MTS Nano Indenter G200, USA). GCr15 bearing steel balls (diameter = 10 mm; hardness = 8.2 GPa) were used as the upper balls sliding against 45 steel and Q45 steel substrates.

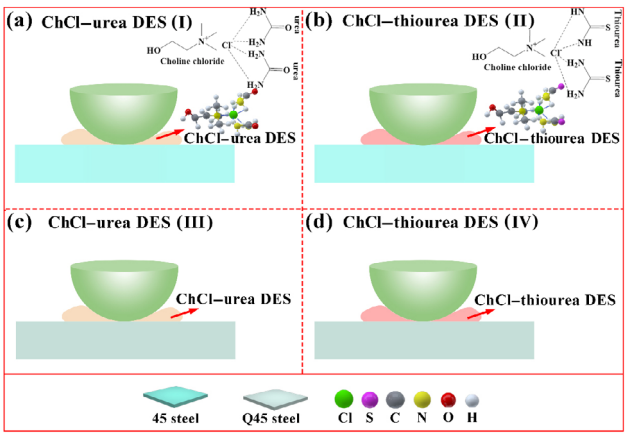

Fig. 1 Framework illustration of the tribological experiments

Table 1 Used substrates, HBA, HBD, and corresponding naming of two DESs in this work.

No.	HBA	HBD	Substrate
ChCl–urea DES (I)	Choline chloride (ChCl)	Urea	45 steel
ChCl–thiourea DES (II)	Choline chloride (ChCl)	Thiourea	45 steel
ChCl–urea DES (III)	Choline chloride (ChCl)	Urea	Q45 steel
ChCl–thiourea DES (IV)	Choline chloride (ChCl)	Thiourea	Q45 steel

The test conditions were as follows: normal load = 50 N; oscillation frequency = 5 Hz; amplitude = 500 μm; number of cycles = 10,000; relative humidity = 50%–60%; and ambient temperature. At least three repetitions were performed. Following the wear experiments, an optical microscope (Motic microscope BA310, China) was used to examine the morphology and dimension of the wear scars. The three-dimensional (3D) profiles and wear volumes of the wear surfaces were analyzed using a 3D optical microscope (Bruker Contour GT-K, Germany).

2.4 Analysis of worn surfaces

The friction mechanism was studied by characterizing the morphology and elemental distribution of the wear tracks using a scanning electron microscope (SEM; FEI Nova 400 FEG-SEM, USA) equipped with an energy-dispersive spectrometer (EDS). The chemical states of the elements within the transfer film on the wear tracks were determined by the X-ray photoelectron spectroscope (XPS; Thermo Scientific ESCALAB 250 Xi, USA). To further elucidate the evolution of the lubrication mechanism of DESs for different tribo-pairs, the distribution of von Mises stress between them was determined by the finite element analysis using ABAQUS software.

3 Results

3.1 Structure of DESs

FTIR spectra of ChCl–urea and ChCl–thiourea DESs with the characteristic bands, along with their vibrational assignments, are shown in Fig. 2 and the results are summarized in Table 2 and Table 3.

Figures 2(a_1)–2(c_1) show the FTIR spectra of ChCl, urea, and ChCl–urea DES, respectively. The vibrational bands at 3,443, 3,360, and 3,210 cm^{-1} correspond to $\nu_{as}NH_2$, ν_sNH_2, and δ_sNH_2 in urea, respectively. However, these bands shifted to 3,430, 3,337, and 3,202 cm^{-1}, respectively, for ChCl–urea DES, indicating hydrogen bonding between urea and choline [23, 24]. Due to the formation of intermolecular hydrogen bonds between urea and ChCl, the δ_sNH_2 at 1,670 cm^{-1} and $\delta_{as}NH_2$ at 1,624 cm^{-1} in the FTIR spectra of urea shifted to 1,663 and 1,623 cm^{-1}, respectively, in the FTIR spectra of ChCl–urea DES [23, 24]. The band at

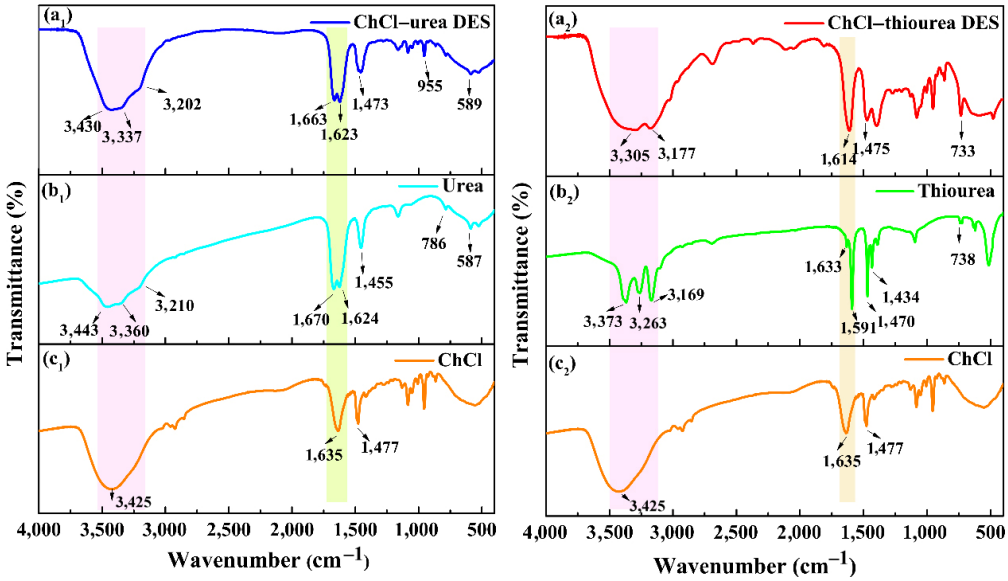

Fig. 2 FTIR spectra of (a_1) ChCl–urea DES, (b_1) urea, and (c_1) ChCl; (a_2) ChCl–thiourea DES, (b_2) thiourea, and (c_2) ChCl.

Table 2 Characteristic band assignments of the FTIR for urea and ChCl–urea DES.

Urea	ChCl–urea DES	Assignments[1]
3,443	3,430	$\nu_{as}NH_2$
3,360	3,337	$\nu_{s}NH_2$
3,210	3,202	$\delta_{s}NH_2$
1,670	1,663	$\delta_{s}NH_2$
1,624	1,623	$\delta_{as}NH_2$
—	1,473	ρCH_3
—	1,161	$\nu_{as}CN$
—	1,081	ρCH_2
1,455	—	$\rho_{s}NH_2$
—	955	$\nu_{as}CCO$
786	786	$\nu_{w}C{=}O$
587	589	δCH
—	524	δCH

1 w = weak; ν = stretching; δ = bending; ρ = rocking; as = asymmetric vibration; s = symmetric vibration.

Table 3 Characteristic band assignments of the FTIR for thiourea and ChCl–thiourea DES.

Thiourea	ChCl–thiourea DES	Assignments[1]
3,373	3,303	$\nu_{s}NH_2$
3,263	—	$\nu_{as}NH_2$
3,169	—	$\nu_{s}NH_2$
1,633	—	$\nu_{as}NH_2$
—	1,614	$\nu_{s}C{=}S$
1,591	—	ν_{as} CN and $\nu_{s}NH_2$
—	1,475	$\nu_{s}C{-}N$
1,470	—	$\nu_{s}N{-}C{-}N$
1,434	—	$\nu_{as}C{=}S$
1,095	—	$\nu_{s}C{-}N$
738	733	$\nu C{=}S$
411	—	$\nu_{s}S{-}C{-}N$

1 ν = stretching; as = asymmetric vibration; s = symmetric vibration.

1,473 cm^{-1} of the ChCl–urea DES that corresponded to CH_3 was associated with ChCl [25]. The existence of νCCO at 955 cm^{-1} in Fig. 2(a_1) indicates that the structure of Ch^+ was retained without being destroyed in ChCl–urea DES [23]. In addition, the band located at 589 cm^{-1} was ascribed to δCH in the ChCl–urea DES [23]. Based on the above results, NH···NH, NH···OH, HO···HO, and OH···NH hydrogen bonds were deemed to be formed in ChCl–urea DES. Similarly, the bands of thiourea located at 3,373, 3,263, and 3,169 cm^{-1} became broader and were assigned to $\nu_{s}NH_2$, $\nu_{as}NH_2$, and $\nu_{s}NH_2$, respectively [26–28]. The ChCl–thiourea DES spectrum (Fig. 2(a_2)) shows bands at 1,614 and 1,475 cm^{-1}, which were attributed to $\nu_{s}C{=}S$ and $\nu_{s}C{-}N$ [28]. The peak at 738 cm^{-1} was assigned to νC=S of thiourea, shifted to low wavenumber (733 cm^{-1}) [27]. The band shift of thiourea indicated the formation of hydrogen bonds between thiourea

and ChCl. Based on the FTIR spectra, it was concluded that both ChCl–urea and ChCl–thiourea DESs were successfully synthesized.

3.2 Thermal stability, viscosity, and wettability of DESs

Melting point is one of the most representative properties of DESs, with their melting point being lower than those of their individual components [15]. Indeed, the melting points of ChCl–urea and ChCl–thiourea DESs are 11.6 and 51.2 °C, respectively, and are far lower than those of their pure components (choline chloride = 302 °C; urea = 133 °C; and thiourea = 176 °C) [14, 26]. In addition to the melting point, the decomposition temperature, kinematic viscosity, and contact angle of the as-synthesized DESs were also measured as key performance metrics, and the results are summarized in Fig. 3 and Table 4. Figure 3(b) show the thermogravimetric (TG) and the differential thermal gravimetric (DTG) curves of the as synthesized DESs. According to the TGA results, ChCl–urea DES began to decompose at approximately 237.7 °C, while the initial decomposition temperature of ChCl–thiourea DES was approximately 223.8 °C. The results indicated that both the synthesized DESs possessed good thermal stability. Viscosity reflects the internal resistance of molecules during fluid flow and affects the ability to form a lubricating film, which is the most significant performance indicator for lubricants [29]. The kinematic viscosity of ChCl–thiourea DES was higher than that of ChCl–urea DES at 80 °C. The affinity of lubricants to the sample surface is assessed by the wettability of the surfaces, which also affects their lubrication performance [19, 30]. Hence, the contact angles were measured to investigate the wettability of the two DESs on 45 steel and Q45 steel at 80 °C, as depicted in Fig. 3. The wetting angle of ChCl–urea DES was lower than that of ChCl–thiourea DES on 45 steel, indicating superior wettability of ChCl–urea DES on 45 steel. However, on Q45 steel, the wettability of ChCl–thiourea DES was better than that of ChCl–urea DES.

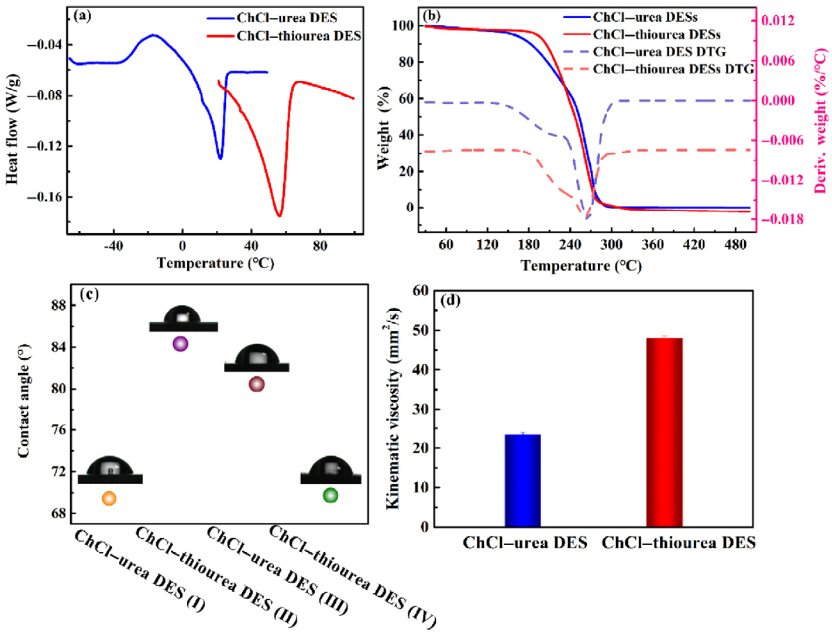

Fig. 3 (a) DSC, (b) TG and DTG curves, (d) kinematic viscosities of ChCl–urea DES and ChCl–thiourea DES, and (c) the photographs and contact angle values of ChCl–urea DES (I), ChCl–thiourea DES (II), ChCl–urea DES (III), and ChCl–thiourea DES (IV).

Table 4 Decomposition temperature, melting point, contact angles on 45 steel and Q45 steel, and the kinematic viscosities of two DESs.

	T_{oneset} (℃)	T_{endset} (℃)	Melting point (℃)	Contact angle on 45 steel (°)	Contact angle on Q45 steel (°)	Kinematic viscosity (mm^2/s)
ChCl–urea DES	237.7	275.4	11.6	69 ± 0.25	83 ± 0.16	23.3 ± 0.64
ChCl–thiourea DES	223.8	275.6	51.2	80 ± 0.04	69 ± 0.13	47.9 ± 0.66

3.3 Friction and wear tests

3.3.1 Effects of DESs on the friction coefficient of GCr15/45 steel and GCr15/Q45 steel pairs

The effects of HBDs on the lubrication effectiveness of DESs were evaluated in comparison with the tribological properties of ChCl–urea and ChCl–thiourea DESs. Figure 4 shows the friction curves of GCr15/45 steel and GCr15/Q45 steel tribo-pairs under ChCl–urea and ChCl–thiourea DESs at 80 °C, labelled as ChCl–urea DES (I), ChCl–thiourea DES (II), ChCl–urea DES (III), and ChCl–thiourea DES (IV).

As shown in Figs. 4(a) and (b), the average friction coefficient of ChCl–thiourea DES (II) was much lower than that of ChCl–urea DES (I) throughout the experiment, indicating that ChCl–thiourea DES has a more positive contribution to the anti-friction effect than ChCl–urea DES for GCr15/45 steel tribo-pairs. The average friction coefficient for ChCl–thiourea DES (II) started at approximately 0.12, but decreased to 0.08 after 2,000 cycles and then stabilized. However, the average friction coefficient for ChCl–urea DES (I) fluctuated around 0.17 for the entire test period.

For the GCr15/Q45 steel tribo-pairs, the average friction coefficients of both DESs fluctuated between 0.08 and 0.12, as shown in Fig. 4. These results imply a similar anti-friction performance of ChCl–urea DES (III) and ChCl–thiourea DES (IV). The average friction coefficient for ChCl–thiourea DES (IV) was higher than that of ChCl–urea DES (III) in the early stages. Then it decreased to 0.08 after approximately 7,000 cycles and remained at 0.08 for the rest of the test.

In summary, the average friction coefficient of the DESs varied with the HBDs.

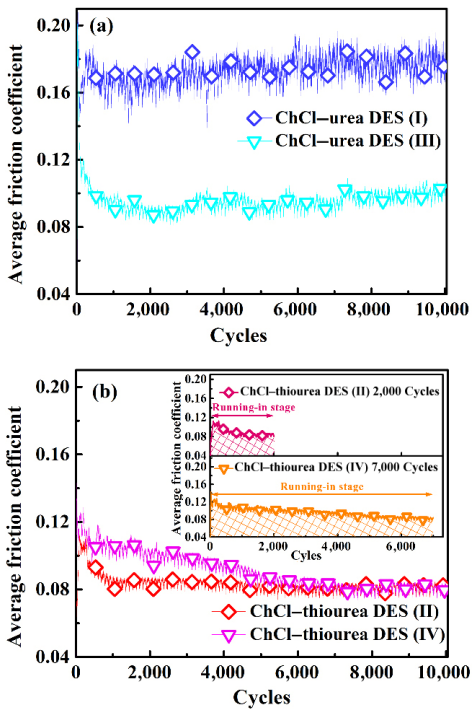

Fig. 4 Friction curves of ChCl–urea DES (I), ChCl–thiourea DES (II), ChCl–urea DES (III), and ChCl–thiourea DES (IV).

3.3.2 Effects of substrates on the friction coefficient of tribo-pairs under DESs

The influence of the mechanical properties of the substrates on the tribological performance of the DESs was also investigated. Prior to the friction experiments, the hardness and elastic modulus of the substrates were measured using nanoindentation tests, as shown in Fig. 5. After quenching, the nano-hardness of 45 steel increased from 2.0 to 15.4 GPa, while the elastic modulus decreased from 331.7 to 212.7 GPa. Thus, Q45 steel possesses better wear resistance owing to the higher nano-hardness to elastic modulus (H/E) ratio [31].

The average friction coefficient curves for ChCl–urea DES (III) and ChCl–urea DES (I) are shown in Fig. 4. ChCl–urea DES (III) exhibited a lower friction coefficient than ChCl–urea DES (I), implying excellent anti-friction performance of ChCl–urea DES for the GCr15/Q45 steel friction pairs. However, the evolution of the friction coefficient for both ChCl–thiourea DES (II) and ChCl–thiourea DES (IV) was similar. The average friction coefficient values were 0.12 during the initial stage and then gradually decreased to 0.08 and eventually stabilized there. The running-in

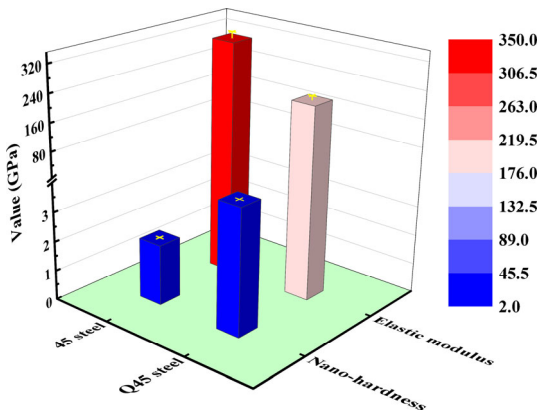

Fig. 5 Nano indentation test results of 45 steel and Q45 steel.

period of ChCl–thiourea DES (II) was shorter than that of ChCl–thiourea DES (IV). The above results demonstrated that the tribological behavior of the GCr15/45 steel tribo-pairs under the DESs was significantly affected by the mechanical properties of the 45 steel.

3.3.3 Effects of DESs on the wear rate of GCr15/45 steel and GCr15/Q45 steel pairs

The cross-sectional profiles, wear volume, and wear rate for ChCl–urea DES (I), ChCl–thiourea DES (II), ChCl–urea DES (III), and ChCl–thiourea DES (IV) are shown in Fig. 6. The cross-section profile of the wear track for ChCl–urea DES (I) was wider and deeper than that of ChCl–thiourea DES (II). The wear rate for ChCl–urea DES (I) was 0.0289 $\mu m^3/(N\cdot\mu m)$, which was approximately an order of magnitude higher than that of ChCl–thiourea DES (II) (0.0056 $\mu m^3/(N\cdot\mu m)$), as shown in Fig. 6(b). Figure 7 shows the 3D surface morphologies of the tribo-pairs after the frictional experiments. Figures 7(a) and 7(b) show that the wear damage of the counterpart ball for ChCl–urea DES (I) was more severe than that of ChCl–thiourea DES (II). Figure 7(e) shows the wear of the counterpart ball under

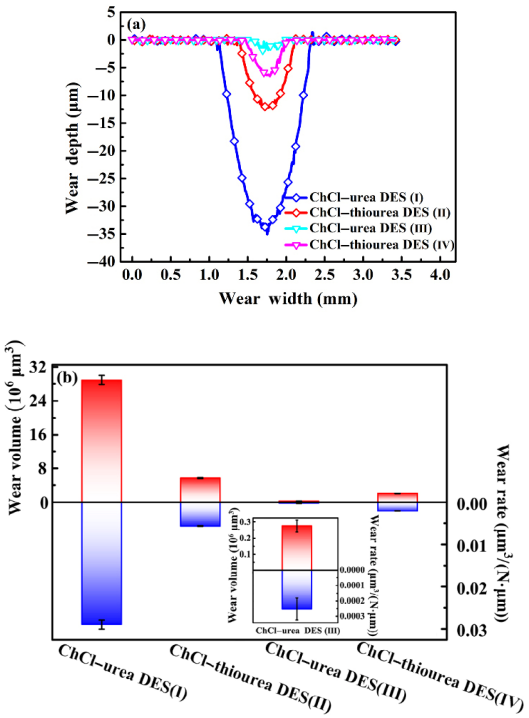

Fig. 6 (a) Cross section profiles and (b) wear volume and wear rate of ChCl–urea DES lubrication (I), ChCl–thiourea DES (II), ChCl–urea DES (III), and ChCl–thiourea DES (IV).

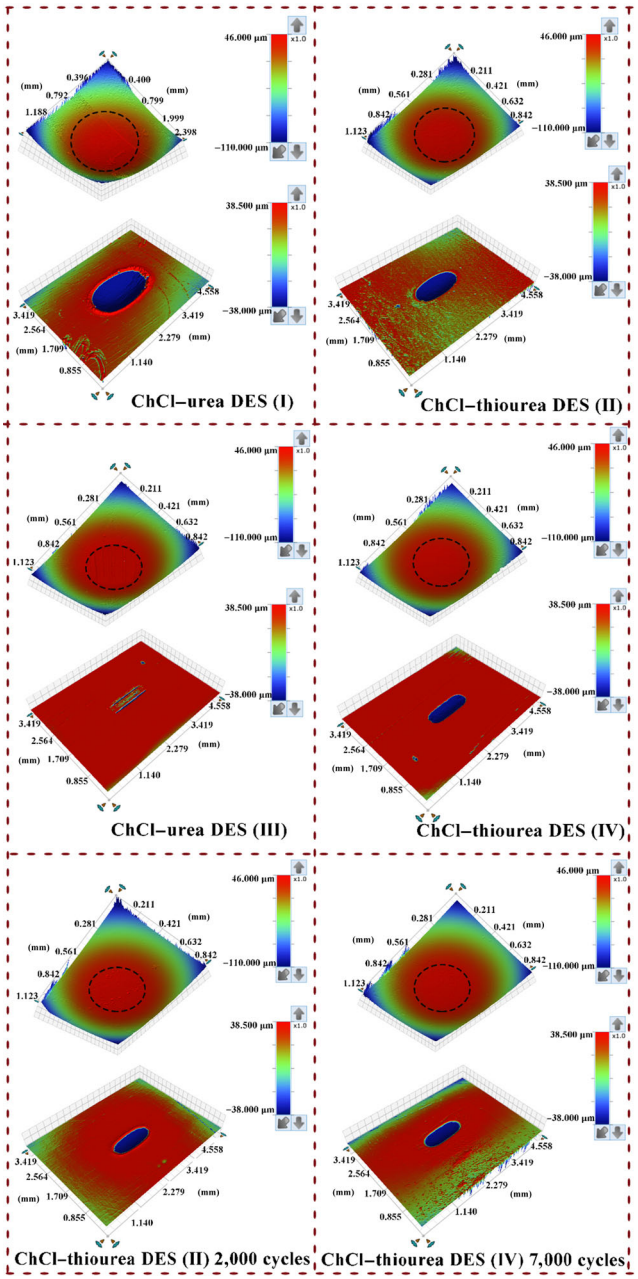

Fig. 7 3D morphologies of friction pairs lubricated by two DESs on 45 steel and Q45 steel.

the ChCl–thiourea DES (II) mainly occurred before 2,000 cycles. Figure 8 shows the optical micrographs of wear scars under ChCl–urea DES (I), ChCl–thiourea DES (II), ChCl–urea DES (III), and ChCl–thiourea DES (IV). The wear scar diameter of the steel ball under ChCl–thiourea DES (II) was relatively smaller than that under ChCl–urea DES (I), as shown in Figs. 8(a) and 8(b). This result was consistent with the findings from the 3D profiles of the balls.

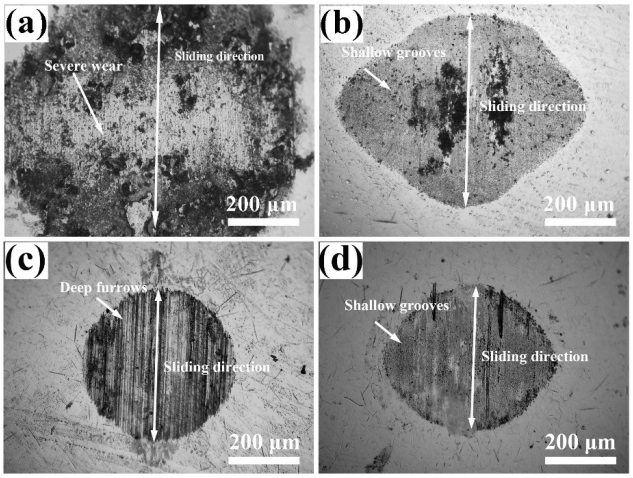

Fig. 8 Optical micrographs of wear scars under (a) ChCl–urea DES lubrication (I), (b) ChCl–thiourea DES (II), (c) ChCl–urea DES (III), and (d) ChCl–thiourea DES (IV).

The wear rate for ChCl–urea DES (III) (0.0003 $\mu m^3/(N\cdot\mu m)$) was lower than that of ChCl–thiourea DES (IV) (0.002 $\mu m^3/(N\cdot\mu m)$). Furthermore, Figs. 7(c) and 7(d) show that the counterpart balls suffered similar wear damage under ChCl–urea DES (III) and ChCl–thiourea DES (IV). The counterpart ball under ChCl–thiourea DES (IV) before 7,000 cycles was severely worn, as shown in Fig. 7(f). As can be seen from Figs. 8(c) and 8(d), the wear scar diameters of ChCl–urea DES (III) and ChCl–thiourea DES (IV) were similar. Along the sliding direction, the wear scar possessed deep grooves under ChCl–urea DES (III) and shallow grooves under ChCl–thiourea DES (IV) due to the abrasive wear.

3.3.4 Effects of the substrates on the wear of the tribo–pairs under DESs

This study not only analyzes the impacts of HBDs on the tribological properties of DESs, but also probes the wear damages of 45 steel and Q45 steel lubricated by DESs. The wear rate for ChCl–urea DES (I) was approximately two orders of magnitude higher than that of ChCl–urea DES (III) because of the superior anti-wear properties of Q45 steel. The wear scar for ChCl–urea DES (I) lubrication displayed a larger diameter than that for ChCl–urea DES (III) (Figs. 8(a) and 8(c), respectively). This can be attributed to the fact that the wear resistance of Q45 steel is higher than that of 45 steel.

In contrast, the wear rate of ChCl–thiourea DES (II) after 10,000 cycles (0.0056 $\mu m^3/(N\cdot\mu m)$) was higher than that of ChCl–thiourea DES (IV) (0.002 $\mu m^3/(N\cdot\mu m)$). Figures 8(b) and 8(d) show that the wear scar diameter for ChCl–thiourea DES (II) after 10,000 cycles was larger than that of ChCl–thiourea DES (IV). The wear volume losses for ChCl–thiourea DES (II) and ChCl–thiourea DES (IV) during the running-in period were also analyzed. The wear volume of ChCl–thiourea DES (II) before 2,000 cycles accounted for approximately 35.5% of the total wear volume (10,000 cycles), and the wear volume of ChCl–thiourea DES (IV) before 7,000 cycles was approximately 0.002 μm^3, accounting for 97.1% of the total wear volume (10,000 cycles). These results indicated that the wear losses of ChCl–thiourea DES (II) and ChCl–thiourea DES (IV) occurred mainly during the running-in period.

3.3.5 Composition of the wear tracks and wear scars

EDS elemental mapping was used to analyze the wear tracks lubricated by ChCl–urea and ChCl–thiourea DESs to elucidate the anti-friction and anti-wear mechanisms on the two steels. As shown in Figs. 9(a) and 9(b), no obvious tribo-chemical reaction was observed in the corresponding EDS mappings of the wear surfaces for ChCl–urea DES (I) and ChCl–urea DES (III). However, ChCl–thiourea DES reacted with the steel substrates to form a tribo-chemical film irrespective of the type of steel substrate, as shown in Figs. 9(c) and 9(d).

To verify the EDS mapping results and further confirm the chemical states of the elements on the wear tracks, XPS was performed, and the results are shown in Figs. 10–13. The XPS spectra of the wear surface under ChCl–urea DES (I) are shown in Fig. 10. The binding energy (BE), full width at half maximum (FWHM), and corresponding peak assignments of the Fe 2p and O 1s peaks are listed in Table 5. Based on fitting peaks of Fe 2p and O 1s, it was determined that FeO, Fe_2O_3, Fe_3O_4, FeOOH, and $FeCl_3$ existed in the wear tracks [32–40]. Figure 11 shows the XPS spectra of the wear tracks under the ChCl–urea DES lubrication with Q45 steel as the substrate. The Fe 2p spectra on the wear tracks were fitted into four peaks at 706.0, 707.0, 709.6, and 711.8 eV (Table 6). According to the XPS peaks of O 1s (at approximately 528.1, 529.7,

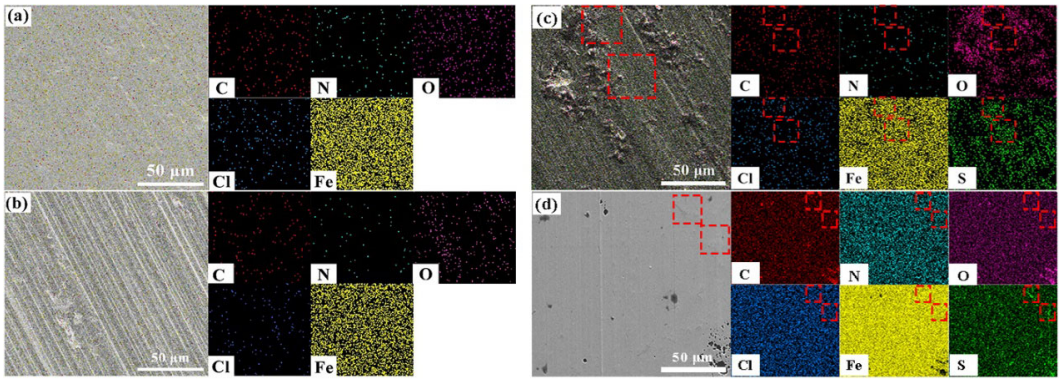

Fig. 9 SEM micrographs and EDS mappings of wear tracks lubricated by (a) ChCl–urea DES (I), (b) ChCl–urea DES (III), (c) ChCl–thiourea DES (II), and (d) ChCl–thiourea DES (IV).

Table 5 Peak position, FWHM and corresponding peaks assignments for Fe 2p and O 1s spectra under ChCl–urea DES (I).

Region	BE (eV)	FWHM (eV)	Assigned to	Ref.
Fe 2p	705.2	1.3	Fe	[53]
	708.3	2.6	Fe_3O_4	[33]
	709.8	2.6	FeO or Fe_3O_4	[33]
	711.8	2.0	Fe_2O_3 or $FeCl_3$ or FeOOH	[33–35]
O 1s	528.1	1.3	O_2	[45]
	529.6	1.4	Fe_2O_3 or FeO or FeOOH	[34, 36–38, 40]
	530.7	2.4	Fe_3O_4	[39]

Table 6 Peak position, FWHM, and corresponding peaks assignments for Fe 2p and S 2p spectra under ChCl–urea DES (III).

Region	BE (eV)	FWHM (eV)	Assigned to	Ref.
Fe 2p	706.0	1.0	Fe	[49]
	707.0	2.1	Fe	[33]
	709.6	2.3	FeO	[33]
	711.8	2.7	$FeCl_3$ or Fe_2O_3 or FeOOH FeOOH	[33–35]
O 1s	528.1	1.2	O_2	[45]
	529.7	1.8	Fe_2O_3 or FeO or FeOOH	[34, 36–40]
	530.9	2.6	Fe_3O_4	[39]

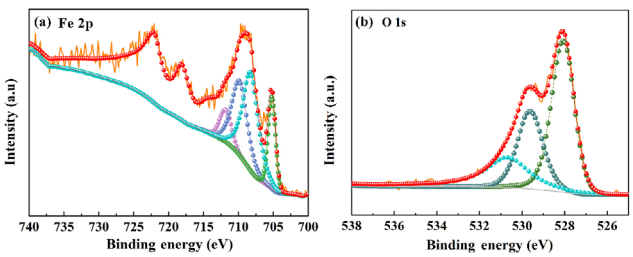

Fig. 10 XPS spectra of (a) Fe 2p and (b) O 1s on the wear surface under ChCl–urea DES (I).

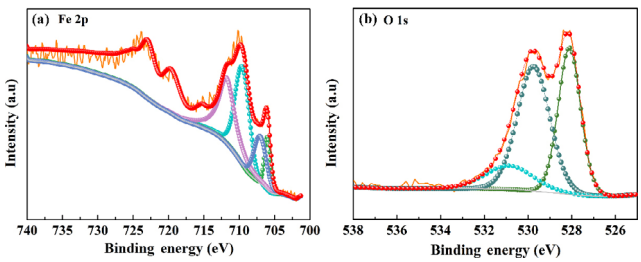

Fig. 11 XPS spectra of (a) Fe 2p and (b) O 1s on the wear surface under ChCl–urea DES (III).

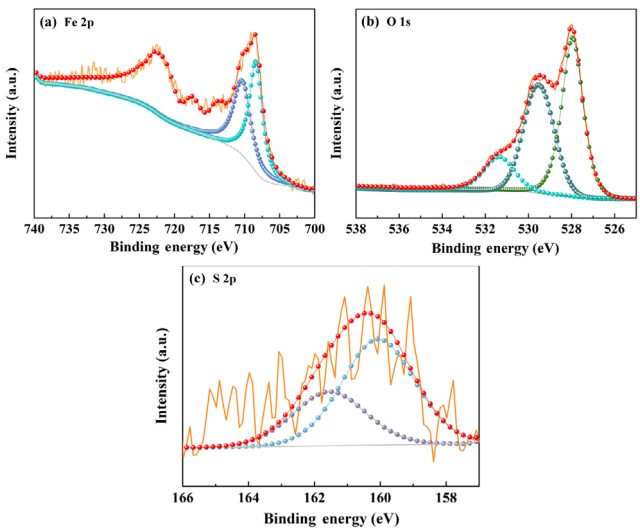

Fig. 12 XPS spectra of (a) Fe 2p, (b) O 1s, and (c) S 2p on the wear surface under ChCl–thiourea DES (II).

and 530.9 eV), this may be attributed to FeO, $FeCl_3$, Fe_2O_3, FeOOH, and Fe_3O_4 [34–44]. The EDS mapping and XPS results of the wear tracks showed that there was no tribo-chemical reaction between ChCl–urea DES and 45 steel or Q45 steel.

The EDS mappings of wear tracks under ChCl–thiourea DES lubrication showed that ChCl–thiourea

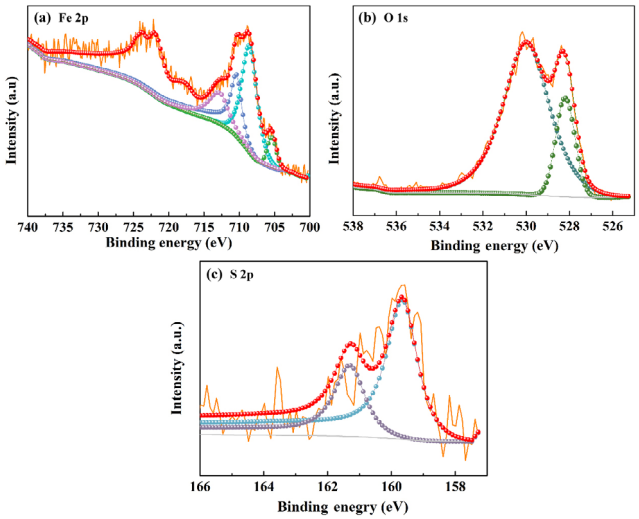

Fig. 13 XPS spectra of (a) Fe 2p, (b) O 1s, and (c) S 2p on the wear surface under ChCl–thiourea DES (IV).

DES reacted with steel substrates during the friction process. The XPS spectra of Fe 2p, O 1s, and S 2p on the wear tracks of ChCl–thiourea DES (II) are shown in Fig. 12 and the results are listed in Table 7. The binding energy signal of the Fe 2p spectrum around 708.4 eV is attributed to Fe_3O_4 in Fig. 12(a) [32]. Specifically, the appearance of the Fe 2p signal (at 710.1 eV) and the corresponding S 2p signal (at 161.6 eV) showed the formation of a tribo-chemical film composed of FeS or FeS_2 [41–45]. These results are consistent with those of EDS mapping analysis. Furthermore, the S 2p observed at 160.3 eV is ascribed to S^{2-}. With Q45 steel as the substrate, the S 2p signals at 159.7 eV and 161.3 eV are assigned to the S^{2-} and FeS, as shown in Fig. 13 and Table 8 [45, 46]. The peaks of O 1s at 528.2 and 530.0 eV are attributed to O_2 and Fe_3O_4 or FeO, respectively [37, 47, 48]. Combined with the S 2p peak at 161.3 eV and Fe 2p peak at 712.5 eV on the wear tracks of Q45 steel, the formation of FeS at the friction interfaces can be confirmed. The Fe 2p spectra are fitted with four signals at 705.5, 708.7, 710.6, and 712.5 eV, corresponding to Fe, FeS_2 or Fe, FeO or Fe_3O_4, and FeS, respectively [33, 43, 49]. Based on the XPS results of ChCl–thiourea DES (II) and ChCl–thiourea DES (IV), the product of the tribo-chemical reactions between ChCl–thiourea DES and substrates was determined to be FeS.

Table 7 Peak position, FWHM, and corresponding peaks assignments for Fe 2p and S 2p spectra under ChCl–thiourea DES (II).

Region	BE (eV)	FWHM (eV)	Assigned to	Ref.
Fe 2p	708.4	2.2	Fe_3O_4	[32]
	710.1	2.9	FeS	[41]
O 1s	528.0	1.2	O_2	[47]
	529.5	1.7	Fe_2O_3 or FeO or FeOOH	[33, 35–39]
	531.3	1.8	Fe_2O_3	[50]
S 2p	160.3	3.4	FeS or S^{2-}	[46, 51]
	161.6	3.4	FeS_2 or FeS	[42, 45]

Table 8 Peak position, FWHM, and corresponding peaks assignments for Fe 2p and S 2p spectra under ChCl–thiourea DES (IV).

Region	BE (eV)	FWHM (eV)	Assigned to	Ref.
Fe 2p	705.5	1.5	Fe	[39]
	708.7	2.6	FeS_2 or Fe	[43, 49]
	710.6	1.9	FeO or Fe_3O_4	[33]
	712.5	3.4	FeS	[52]
O 1s	528.2	1.0	O_2	[47]
	530.0	2.6	Fe_3O_4 or FeO	[35, 36, 48]
S 2p	159.7	1.3	S^{2-}	[46]
	161.3	1.1	FeS	[35]

4 Discussion

4.1 Influence of HBDs in DESs on the tribological behavior of the GCr15/45 steel tribo-pairs

According to the XPS and EDS mapping results, ChCl–thiourea DES reacted with the fresh Fe surface to form a tribo-chemical film consisting of FeS. The tribo-chemical film played an important role in friction-reducing and anti-wear properties. Therefore, the friction coefficient and wear rate for ChCl–thiourea DES (II) were lower than those for ChCl–urea DES (I). It can be concluded that the formation of the lubrication film is associated with the HBDs in the DESs. Thiourea in ChCl–thiourea DES contains an active sulfur element that can react with friction interfaces to form a protective film. This further indicates that the selection of HBDs containing an active element contributes to improving the lubrication effect of the DESs.

4.2 Effects of HBDs in DESs on the tribological properties of the GCr15/Q45 steel tribo-pairs

Interestingly, the sulfur-containing HBD failed to improve the lubrication effect as the hardness of the substrate increased. As shown in Fig. 6, the wear rate of ChCl–thiourea DES (IV) was higher than that of ChCl–urea DES (III). To probe the tribological mechanism, the distribution of von Mises stress between the wear track and the counterpart ball was analyzed using ABAQUS software. The distribution of von Mises stress in the direction perpendicular to the wear track and the cross-sectional profiles of the wear tracks under ChCl–thiourea DES (II) and ChCl–thiourea DES (IV) are shown in Fig. 14. The von Mises stress closer to the edge of the wear track was much higher than that in the center of the wear track. In addition, the von Mises stress decreased with the widening and deepening of the wear track. As demonstrated in this study, the Q45 steel showed good wear resistance, and thus, the wear tracks of Q45 steel were shallow. Consequently, the von Mises stress for the wear tracks of the Q45 steel was high, as shown in Fig. 14(b). It is reasonable to postulate that the absence of a tribo-chemical reaction film in the wear track for ChCl–thiourea (IV) during the running-in period is due to the high von Mises stress between friction interfaces, as shown in Fig. 15. The tribo-chemical reaction film peels from the contact interfaces under high von Mises stress, leading to the wear of Q45 steel during the running-in period. Then, the fresh surface of Q45 steel that is produced by scratching reacts with ChCl–thiourea DES to form a lubrication film, which is peeled from the contact interfaces again. This process is repeated until the end of the running-in period. A schematic of ChCl–thiourea DES (IV) is shown in Fig. 16(b). The wear rate for ChCl–thiourea DES (IV) was higher than that of ChCl–urea DES (III), and the wear volume of ChCl–thiourea DES (IV) before 7,000 cycles accounted for 97.1% of the total wear volume (10,000 cycles).

Notably, the von Mises stress corresponding to the wear track of ChCl–thiourea (II) after 2,000 cycles was the same as that of ChCl–thiourea (IV) after 7,000 cycles, with the minimum von Mises stress on the wear tracks being 2,670 MPa. According to Fig. 4, the steady-state friction coefficients for ChCl–thiourea DES (II) at the 2,000th cycle and ChCl–thiourea (IV) at the 7,000th cycle were low. The steady-state friction coefficient can be derived from the low von Mises

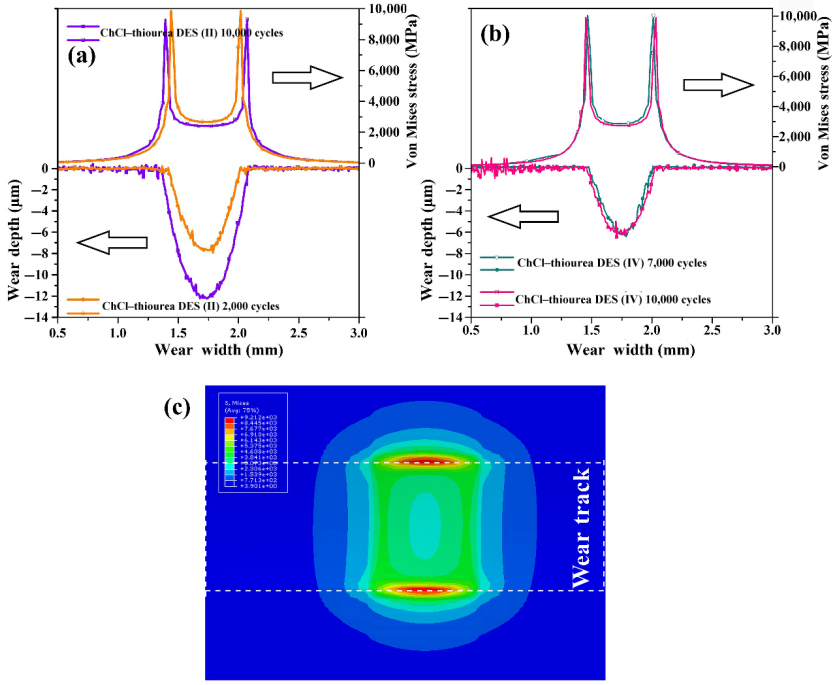

Fig. 14 Cross section profiles and von Mises Stress of the wear traces (a) on 45 steel and (b) on Q45 steel lubricated by ChCl–thiourea DES during running-in stage and entire experiments. (c) Stress distribution of the wear traces for ChCl–thiourea DES (IV) after 10,000 cycles.

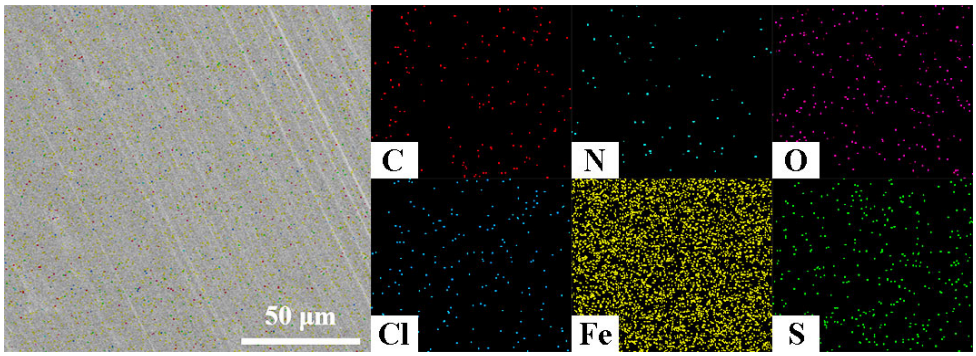

Fig. 15 SEM micrograph and EDS mappings of wear tracks for ChCl–thiourea DES (IV) during running-in period.

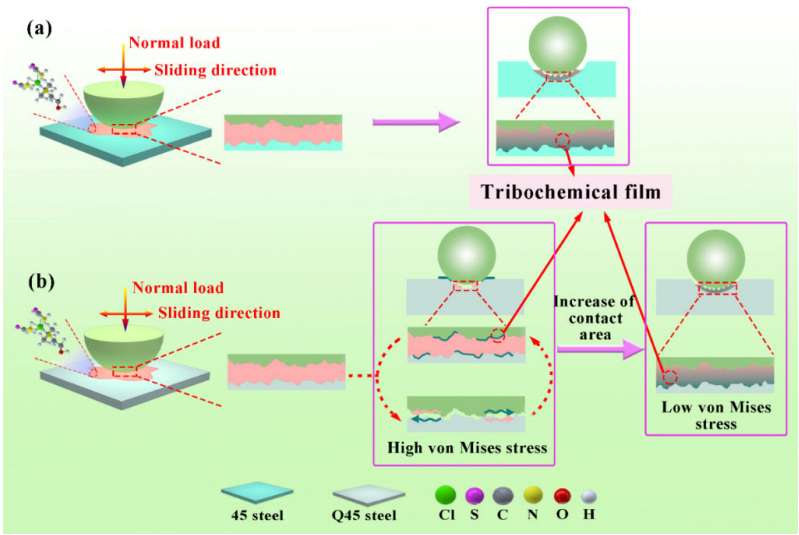

Fig. 16 Schematic diagrams of (a) ChCl–thiourea DES (II) and (b) ChCl–thiourea DES (IV).

stress, and it can be obtained only when the von Mises stress is lower than a certain value. The von Mises stress of ChCl–thiourea DES (IV) decreased with increasing contact area between rubbing interfaces as the experiment progressed. Thus, the lubrication film could be retained at the interface in the steady state, reducing friction and preventing undesirable wear of the interfaces in the region of low von Mises stress, as shown in Fig. 16(b). Hence, the average friction coefficient of ChCl–thiourea DES (IV) gradually decreased to 0.08 after 7,000 cycles. The stable average friction coefficient of ChCl–thiourea DES (IV) was lower than that of ChCl–urea DES (III).

4.3 Tribological properties of GCr15/45 steel and GCr15/Q45 steel tribo-pairs under ChCl–urea DES

According to the EDS mappings and XPS spectra, there is no tribo-chemical reaction between the ChCl–urea DES and the friction interfaces. However, due to the higher H/E of Q45 steel, the average friction coefficient for ChCl–urea DES (III) was lower than that for ChCl–urea DES (I) [40, 53]. For the same reason, the better wear resistance of Q45 steel was illustrated by the lower wear rate and wear scar diameter for ChCl–urea DES (III) than those of ChCl–urea DES (I) [31].

4.4 Tribological properties of GCr15/45 steel and GCr15/Q45 steel tribo-pairs under ChCl–thiourea DES

Similarly, when sliding under ChCl–thiourea DES lubrication, the wear rate of 45 steel was slightly higher than that of Q45 steel, as 45 steel was more prone to wear. Thus, the contact area between the 45 steel and the counterpart ball quickly increased owing to the

increased wear of 45 steel, leading to a sharp decrease in the von Mises stress, as shown in Fig. 14. The steady state could be reached after a short running-in period. Therefore, the tribo-chemical film on the wear surfaces could be retained in the contact interface to reduce friction and wear. A schematic of ChCl–thiourea DES (II) is shown in Fig. 16(a). However, as discussed in Section 4.2, the formed tribo-chemical film is readily peeled from the friction interface owing to the excellent wear resistance of Q45 steel under high von Mises stress. In the steady state, the film could be retained in the sliding interfaces at lower von Mises stress, thereby providing a lubrication effect, as shown in the low von Mises stress state in Fig. 16(b). Consequently, the average friction coefficient of ChCl–thiourea DES on 45 steel was stable at 0.08 after 2,000 cycles, while on Q45 steel, it stayed at 0.08 even after 7,000 cycles. It can be summarized that a stable tribo-chemical film is not easily formed between the friction interfaces under high von Mises stress, leading to the decreased effective lubrication effect.

5 Conclusions

ChCl–urea and ChCl–thiourea DESs with good thermal stabilities were successfully synthesized by heating and stirring ChCl with urea and thiourea, respectively. Their lubrication performances were investigated systematically. The main conclusions are summarized as follows:

1) For GCr15/45 steel pairs, the as-synthesized ChCl–thiourea DES containing active S could react with the steel substrate to form an FeS lubrication film, leading to low friction coefficient and wear rate.

2) For GCr15/Q45 steel pairs lubricated by ChCl–thiourea DES, the tribo-chemical reaction film could be peeled from the contact interfaces because of the high von Mises stress during the running-in process, leading to higher friction coefficient and wear rate than those of ChCl–urea DES.

3) The wear of Q45 steel lubricated by two DESs was lower than that of 45 steel owing to the higher H/E value.

4) The load-bearing ability of the lubrication film at the rubbing interface is a critical factor governing its anti-friction and anti-wear properties. This study lays the groundwork for future research into the design of DES lubricants.

Acknowledgements

The authors acknowledge the supports from the National Natural Science Foundation of China (No. 51805455), Sichuan Science and Technology Program (Nos. 2019YFG0306 and 2019YFSY0012), and the Fundamental Research Funds for the Central Universities (No. 2682020CX04). We also thank the technical support provided by "Ceshigo Research Service Agency for DSC analysis, www.ceshigo.com" and Analytical and Testing Center of Southwest Jiaotong University for supporting the SEM measurements.

References

[1] Abbott A P, Ahmed E I, Harris R C, Ryder K S. Evaluating water miscible deep eutectic solvents (DESs) and ionic liquids as potential lubricants. *Green Chem* **16**(9): 4156–4161 (2014)

[2] Zhou Y, Dyck J, Graham T W, Luo H M, Leonard D N, Qu J. Ionic liquids composed of phosphonium cations and organophosphate, carboxylate, and sulfonate anions as lubricant antiwear additives. *Langmuir* **30**(44): 13301–13311 (2014)

[3] Boyde S. Green lubricants. Environmental benefits and impacts of lubrication. *Green Chem* **4**(4): 293–307 (2002)

[4] Hörner D. Recent trends in environmentally friendly lubricants. *J Synth Lubr* **18**(4): 327–347 (2002)

[5] Dugoni G C, di Pietro M E, Ferro M, Castiglione F, Ruellan S, Moufawad T, Moura L, Costa Gomes M F, Fourmentin S, Mele A. Effect of water on deep eutectic solvent/β-cyclodextrin systems. *ACS Sustainable Chem Eng* **7**(7): 7277–7285 (2019)

[6] Zhang K, Ren S H, Yang X, Hou Y C, Wu W Z, Bao Y Y. Efficient absorption of low-concentration SO_2 in simulated flue gas by functional deep eutectic solvents based on imidazole and its derivatives. *Chem Eng J* **327**: 128–134 (2017)

[7] Wagle D V, Zhao H, Baker G A. Deep eutectic solvents: Sustainable media for nanoscale and functional materials. *Acc Chem Res* **47**(8): 2299–2308 (2014)

[8] Adhikari L, Larm N E, Bhawawet N, Baker G A. Rapid microwave-assisted synthesis of silver nanoparticles in a halide-free deep eutectic solvent. *ACS Sustainable Chem Eng* **6**(5): 5725–5731 (2018)

[9] Smith E L, Abbott A P, Ryder K S. Deep eutectic solvents (DESs) and their applications. *Chem Rev* **114**(21): 11060–11082 (2014)

[10] Zhang Q, De Oliveira Vigier K, Royer S, Jérôme F. Deep eutectic solvents: Syntheses, properties and applications. *Chem Soc Rev* **41**(21): 7108–7146 (2012)

[11] Chen Z, Greaves T L, Warr G G, Atkin R. Mixing cations with different alkyl chain lengths markedly depresses the melting point in deep eutectic solvents formed from alkylammonium bromide salts and urea. *Chem Commun* (*Camb*) **53**(15): 2375–2377 (2017)

[12] Weaver K D, Kim H J, Sun J Z, MacFarlane D R, Elliott G D. Cyto-toxicity and biocompatibility of a family of choline phosphate ionic liquids designed for pharmaceutical applications. *Green Chem* **12**(3): 507–513 (2010)

[13] Ilgen F, Ott D, Kralisch D, Reil C, Palmberger A, König B. Conversion of carbohydrates into 5-hydroxymethylfurfural in highly concentrated low melting mixtures. *Green Chem* **11**(12): 1948–1954 (2009)

[14] Li X Y, Hou M Q, Han B X, Wang X L, Zou L Z. Solubility of CO_2 in a choline chloride + urea eutectic mixture. *J Chem Eng Data* **53**(2): 548–550 (2008)

[15] Abbott A P, Capper G, Davies D L, Shikotra P. Processing metal oxides using ionic liquids. *Miner Process Extr Metall* **115**(1): 15–18 (2006)

[16] Morrison H G, Sun C C, Neervannan S. Characterization of thermal behavior of deep eutectic solvents and their potential as drug solubilization vehicles. *Int J Pharm* **378**(1–2): 136–139 (2009)

[17] Abbott A P, Cullis P M, Gibson M J, Harris R C, Raven E. Extraction of glycerol from biodiesel into a eutectic based ionic liquid. *Green Chem* **9**(8): 868–872 (2007)

[18] Karam A, Villandier N, Delample M, Koerkamp C K, Douliez J P, Granet R, Krausz P, Barrault J, Jérôme F. Rational design of sugar-based-surfactant combined catalysts for promoting glycerol as a solvent. *Chem A Eur J* **14**(33): 10196–10200 (2008)

[19] Lawes S D A, Hainsworth S V, Blake P, Ryder K S, Abbott A P. Lubrication of steel/steel contacts by choline chloride ionic liquids. *Tribol Lett* **37**(2): 103–110 (2010)

[20] Shi Y J, Mu L W, Feng X, Lu X H. Friction and wear behavior of CF/PTFE composites lubricated by choline chloride ionic liquids. *Tribol Lett* **49**(2): 413–420 (2013)

[21] Antunes M, Campinhas A S, de Sá Freire M, Caetano F, Diogo H P, Colaço R, Branco L C, de Saramago B. Deep eutectic solvents (DES) based on sulfur as alternative lubricants for silicon surfaces. *J Mol Liq* **295**: 111728 (2019)

[22] Hallett J E, Hayler H J, Perkin S. Nanolubrication in deep eutectic solvents. *Phys Chem Chem Phys* **22**(36): 20253–20264 (2020)

[23] Yue D Y, Jia Y Z, Yao Y, Sun J H, Jing Y. Structure and electrochemical behavior of ionic liquid analogue based on choline chloride and urea. *Electrochimica Acta* **65**: 30–36 (2012)

[24] Delgado-Mellado N, Larriba M, Navarro P, Rigual V, Ayuso M, García J, Rodríguez F. Thermal stability of choline chloride deep eutectic solvents by TGA/FTIR–ATR analysis. *J Mol Liq* **260**: 37–43 (2018)

[25] Yuan C S, Zhang X, Ren Y F, Feng S Q, Liu J B, Wang J, Su L. Temperature- and pressure-induced phase transitions of choline chloride–urea deep eutectic solvent. *J Mol Liq* **291**: 111343 (2019)

[26] Madhurambal G, Mariappan M, Mojumdar S C. Thermal, UV and FTIR spectral studies of urea–thiourea zinc chloride single crystal. *J Therm Anal Calorim* **100**(3): 763–768 (2010)

[27] Madhurambal G, Mariappan M, Ravindran B, Mojumdar S C. Thermal and FTIR spectral studies in various proportions of urea thiourea mixed crystal. *J Therm Anal Calorim* **104**(3): 885–891 (2011)

[28] Karimi M, Dadfarnia S, Haji Shabani A M. Hollow fibre-supported graphene oxide nanosheets modified with a deep eutectic solvent to be used for the solid-phase microextraction of silver ions. *Int J Environ Anal Chem* **98**(2): 124–137 (2018)

[29] Pandey A, Pandey S. Solvatochromic probe behavior within choline chloride-based deep eutectic solvents: Effect of temperature and water. *J Phys Chem B* **118**(50): 14652–14661 (2014)

[30] Bombard A J F, Gonçalves F R, Shahrivar K, Ortiz A L, de Vicente J. Tribological behavior of ionic liquid-based magnetorheological fluids in steel and polymeric point contacts. *Tribol Int* **81**: 309–320 (2015)

[31] Leyland A, Matthews A. On the significance of the *H*/*E* ratio in wear control: A nanocomposite coating approach to optimised tribological behaviour. *Wear* **246**(1–2): 1–11 (2000)

[32] McIntyre N S, Zetaruk D G. X-ray photoelectron spectroscopic studies of iron oxides. *Anal Chem* **49**(11): 1521–1529 (1977)

[33] Mills P, Sullivan J L. A study of the core level electrons in iron and its three oxides by means of X-ray photoelectron spectroscopy. *J Phys D*: *Appl Phys* **16**(5): 723–732 (2000)

[34] Kim Y I, Hatfield W E. Electrical, magnetic and spectroscopic properties of tetrathiafulvalene charge transfer compounds with iron, ruthenium, rhodium and iridium halides. *Inorganica Chimica Acta* **188**(1): 15–24 (1991)

[35] Brion D. Etude par spectroscopie de photoelectrons de la degradation superficielle de FeS_2, $CuFeS_2$, ZnS et PbS a l'air et dans l'eau. *Appl Surf Sci* **5**(2): 133–152 (1980) (In French)

[36] McIntyre N S, Zetaruk D G. X-ray photoelectron spectroscopic studies of iron oxides. *Anal Chem* **49**(11): 1521–1529 (1977)

[37] Rueda F, Mendialdua J, Rodriguez A, R Casanova, Barbaux Y, Gengembre L, Jalowiecki L. Characterization of Venezuelan laterites by X-ray photoelectron spectroscopy. *J Electron Spectrosc Relat Phenom* **82**(3): 135–143 (1996)

[38] Marcus P, Grimal J M. The anodic dissolution and passivation of NiCrFe alloys studied by ESCA. *Corros Sci* **33**(5): 805–814 (1992)

[39] Tan B J, Klabunde K J, Sherwood P M A. X-ray photoelectron spectroscopy studies of solvated metal atom dispersed catalysts. Monometallic iron and bimetallic iron–cobalt particles on alumina. *Chem Mater* **2**(2): 186–191 (1990)

[40] Zhou Y F, Li L L, Shao W, Chen Z H, Wang S F, Xing X L, Yang Q X. Mechanical and tribological behaviors of Ti-DLC films deposited on 304 stainless steel: Exploration with Ti doping from micro to macro. *Diam Relat Mater* **107**: 107870 (2020)

[41] Carver J C, Schweitzer G K, Carlson T A. Use of X-ray photoelectron spectroscopy to study bonding in cr, mn, Fe, and co compounds. *J Chem Phys* **57**(2): 973–982 (1972)

[42] Laajalehto K, Kartio I, Nowak P. XPS study of clean metal sulfide surfaces. *Appl Surf Sci* **81**(1): 11–15 (1994)

[43] Panzmer G, Egert B. The bonding state of sulfur segregated to α-iron surfaces and on iron sulfide surfaces studied by XPS, AES and ELS. *Surf Sci* **144**(2–3): 651–664 (1984)

[44] Hawn D D, DeKoven B M. Deconvolution as a correction for photoelectron inelastic energy losses in the core level XPS spectra of iron oxides. *Surf Interface Anal* **10**(2–3): 63–74 (1987)

[45] Becker K H, Haaks D. Measurement of the natural lifetimes and quenching rate constants of OH ($^2\Sigma^+$, v = 0,1) and OD ($^2\Sigma^+$, v = 0,1) radicals. *Zeitschrift Für Naturforschung A* **28**(2): 249–256 (1973)

[46] Yu X R, Liu F, Wang Z Y, Chen Y. Auger parameters for sulfur-containing compounds using a mixed aluminum–silver excitation source. *J Electron Spectrosc Relat Phenom* **50**(2): 159–166 (1990)

[47] Bare S R, Griffiths K, Lennard W N, Tang H T. Generation of atomic oxygen on Ag(111) and Ag(110) using NO_2: A TPD, LEED, HREELS, XPS and NRA study. *Surf Sci* **342**(1–3): 185–198 (1995)

[48] Allen G C, Curtis M T, Hooper A J, Tucker P M. ChemInform abstract: X-ray photoelectron spectroscopy of iron–oxygen systems. *Chemischer Informationsdienst* **5**(41) (1974)

[49] Siriwardane R V, Cook J M. Interactions of SO_2 with sodium deposited on silica. *J Colloid Interface Sci* **108**(2): 414–422 (1985)

[50] Paparazzo E. XPS and auger spectroscopy studies on mixtures of the oxides SiO_2, Al_2O_3, Fe_2O_3 and Cr_2O_3. *J Electron Spectrosc Relat Phenom* **43**(2): 97–112 (1987)

[51] Kutty T R N. A controlled copper-coating method for the preparation of ZnS: Mn DC electroluminescent powder phosphors. *Mater Res Bull* **26**(5): 399–406 (1991)

[52] Binder H, Fischer R. The reaction between boron trifluoride and tertiary phosphites. *Zeitschrift Für Naturforschung B* **27**(7): 753–759 (1972) (In German)

[53] Ho W Y, Chen M D, Lin C L, Ho W Y. Characteristics of TiVN and TiVCN coatings by cathodic arc deposition. In: Proceedings of the 6th International Conference on Mechatronics, Materials, Biotechnology and Environment, Yinchuan, China, 2016: 597–601.

Yuting LI. She is currently a Ph.D. candidate at the School of Materials Science and Engineering, Southwest Jiaotong University, China. Her research interests include the design of lubricating materials and tribological properties of novel deep eutectic solvents.

Yuan LI. He is studying for his Ph.D. degree in Southwest Jiaotong University, China. He received his B.S. degree in 2020 from Hunan University of Science and Technology, China. His research field mainly includes the solid–liquid phase transition of deep eutectic solvent in friction process.

Hao LI. He is currently an instructor at Southwest Jiaotong Unversity, China. He received his Ph.D. degree from Lanzhou Institute of Chemical Physics, Chinese Academy of Sciences, China, in 2016. He received his B.S. degree in 2011 from Lanzhou University. His research interests cover the solid lubricating coatings and the related tribological properties.

Xiaoqiang FAN. He is currently an associate professor at Southwest Jiaotong Unversity, China. He received his Ph.D. degree from Lanzhou Institute of Chemical Physics, Chinese Academy of Sciences, China, in 2016. He received his B.S. degree in 2011 from Qingdao University of Science & Technology, China. His research focuses on the lubricating materials, corrosion protection, and engineering applications. He has published over 50 papers in international journals.

Han YAN. He is currently a Ph.D. candidate at Southwest Jiaotong University, China. He received his B.S. degree in 2016 from Chengdu University of Technology, China His research focuses on the corrosion and tribology fields.

Meng CAI. He received his B.S. degree from Southwest University of Science and Technology, China, in 2018. He is currently a Ph.D. candidate at the School of Mechanical Engineering, Southwest Jiaotong University, China. His research interests include the design of anticorrosion materials for epoxy resin and tribological properties of composite epoxy resin coatings.

Xiaojun XU. He is currently an associate professor at Southwest Jiaotong Unversity, China. He received his Ph.D. degree from Delft University of Technology, the Netherlands, in 2016. His main research interests include the microstructure and properties of high-performance metal materials and service performance of materials.

Minhao ZHU. He received his B.S. and M.S. degrees from Southwest Jiaotong University, Sichuan, China, in 1990 and 1993, respectively. In 2001, he received his Ph.D. degree from Southwest Jiaotong University, China. His current position is a professor, doctoral supervisor, and dean of the School of Materials Science and Engineering in Southwest Jiaotong University, China. His research areas cover the fretting wear, fretting fatigue, surface engineering and design of fastener connection. He has published over 200 papers in international journals such as *Carbon*, *Tribology International*, *Surface & Coatings Technology*, *Tribology Letters*, and *Wear and Friction*.